
Understanding and constraining the PDF uncertainties in a W boson mass measurement with LHCb

Stephen Farry¹, Olli Lupton², Martina Pili³, Mika Vesterinen².

¹*University of Liverpool, Liverpool, United Kingdom*

²*University of Warwick, Coventry, United Kingdom*

³*University of Oxford, Oxford, United Kingdom*

Abstract

Precision electroweak tests are a powerful probe of physics beyond the Standard Model, but the sensitivity is limited by the precision with which the W boson mass (M_W) has been measured. The Parton Distribution Function (PDF) uncertainties are a potential limitation for measurements of M_W with LHC data. It has recently been pointed out that, thanks to LHCb's unique forward rapidity acceptance, a new measurement of M_W by LHCb can improve this situation. While the measurement of M_W by LHCb would also be susceptible to uncertainties in the PDFs, there would be a partial cancellation of the overall PDF uncertainty when the LHCb result is included in an average with measurements by ATLAS and CMS. Here we report on a detailed study on the mechanism driving the PDF uncertainty in the LHCb measurement of M_W , and propose an approach which should reduce this uncertainty by roughly a factor of two using LHCb Run 2 data.

Contents

1	Introduction	1
2	Simulation of W production	2
3	Fitting method	3
4	Importance of PDF regions	4
5	The role of the W kinematics	5
6	PDF uncertainty reduction	9
7	Simultaneous fit of W^+ and W^- samples	10
8	Dependence on the detector acceptance	12
9	Conclusions	14
	References	15
	Additional material	16

1 Introduction

Global fits to precision electroweak data are sensitive to physics beyond the Standard Model (SM). Of notable interest is the mass of the W boson (M_W) because, currently, it is predicted with higher precision than it is measured. The 2018 update of the electroweak fit by the gFitter collaboration indirectly predicts $M_W = 80354 \pm 7 \text{ MeV}/c^2$ [1]. This prediction is more precise than the average of direct measurements reported by the Particle Data Group, $M_W = 80379 \pm 12 \text{ MeV}/c^2$ [2], which is dominated by measurements using $W \rightarrow \ell \nu_\ell$ decays at hadron collider experiments.

Measurements of M_W at hadron colliders are performed by comparing data to templates of the charged lepton transverse momentum, missing transverse energy, and transverse mass in samples of $W \rightarrow \ell \nu_\ell$ decays. The combination of measurements by the CDF [3] and D0 [4] experiments at the Fermilab Tevatron $p\bar{p}$ collider is $M_W = 80387 \pm 16 \text{ MeV}/c^2$ [5]. In $p\bar{p}$ collisions W bosons are primarily produced by the annihilation of valence quarks and antiquarks. By contrast, gluons and sea quarks play a critical role in the pp collisions at the LHC. Measurements of M_W at the LHC are therefore expected to be more susceptible to theoretical uncertainties in the modeling of W production, in particular those related to the Parton Distribution Functions (PDFs), than at the Tevatron [6–10]. ATLAS reported a measurement of $M_W = 80370 \pm 13 \pm 14 \text{ MeV}/c^2$ where the first and second uncertainties are experimental and theoretical, respectively [11]. The dominant contribution to the theoretical uncertainty can be attributed to the PDFs. A key challenge of future measurements by ATLAS and CMS will be to reduce the PDF uncertainty.

The current ATLAS and CMS detectors are capable of reconstructing charged leptons in the approximate pseudorapidity range $|\eta| < 2.5$, where $\eta = -\ln(\tan(\theta/2))$ with θ being the angle between the particle direction and the beam axis. LHCb [12] is a single-arm spectrometer with full charged particle tracking and identification capabilities over the range $2 < \eta < 5$, which is mostly orthogonal to the acceptance of ATLAS and CMS. While LHCb is primarily designed for the study of beauty and charm hadrons, it has a strong track record in measurements of W and Z production in muonic final states [13, 14]. As for precision electroweak tests, LHCb has already measured the effective weak mixing angle $\sin^2 \theta_{\text{eff}}^{\text{lept}}$ [15], but the potential for a measurement of M_W was not realised until recently.

Ref. [16] proposed a new measurement of M_W by LHCb based on the muon transverse momentum (p_T) distribution with $W \rightarrow \mu\nu$ decays. Fig. 1 shows how the shape of the p_T distribution varies with the M_W hypothesis in simulated events. The maximum variation in the normalised distribution, which occurs at $p_T \sim 42 \text{ GeV}/c$, is around 10^{-4} per MeV of shift in M_W . Large W samples are therefore required to resolve this subtle change in the shape of the p_T distribution. After the successful completion of LHCb Run 2 roughly 6 fb^{-1} of pp collisions at $\sqrt{s} = 13 \text{ TeV}$ have been recorded, complementing the 3 fb^{-1} recorded at lower \sqrt{s} values in Run 1. Using the methods described in this paper we estimate that the Run 2 data could yield a M_W measurement with a statistical uncertainty of roughly $10 \text{ MeV}/c^2$. The obvious next question is how well the theoretical uncertainties, in particular those related to the PDFs, can be controlled. Ref. [16] estimated that the PDF uncertainties in a standalone LHCb measurement would be larger than those in ATLAS and CMS. However, the uncertainty on the LHCb measurement would be partially anticorrelated with those of ATLAS and CMS. It is therefore claimed that the introduction of a LHCb measurement into a LHC M_W average could improve the overall PDF uncertainty. Similar improvements may be possible with the extended angular coverage of the ATLAS and CMS upgrade detectors in the HL-LHC era, as explored in a recent study by ATLAS [17]. Given the large size of the LHCb Run 2 dataset, and anticipated future data with LHCb Upgrade I [18] and the proposed Upgrade II [19], it seems worthwhile to study in greater detail the cause of the PDF uncertainty in a measurement of M_W by LHCb, and possible strategies to reduce it.

2 Simulation of W production

A sample of 10^8 Monte Carlo events of the type $pp \rightarrow W \rightarrow \mu\nu + X$, at a centre-of-mass energy $\sqrt{s} = 13 \text{ TeV}$, is generated using POWHEG [20] with the CT10 [21] PDFs. These events are subsequently processed with PYTHIA [22] to simulate the parton showering. No LHCb detector response is simulated. Unless otherwise specified, events are analysed if they satisfy $30 < p_T < 50 \text{ GeV}/c$ and $2 < |\eta| < 4.5$ ¹. Roughly 10% of the initial event sample falls into this kinematic region. The invariant mass of the W decay products (m) is assumed to follow a relativistic Breit-Wigner distribution:

$$\frac{d\sigma}{dm} \propto \frac{1}{(m^2 - M_W^2)^2 + m^4 \Gamma_W^2 / M_W^2}, \quad (1)$$

¹The $2 < |\eta| < 4.5$ selection is chosen to make better use of the available samples: the events falling in that region are equivalently treated as those with positive η .

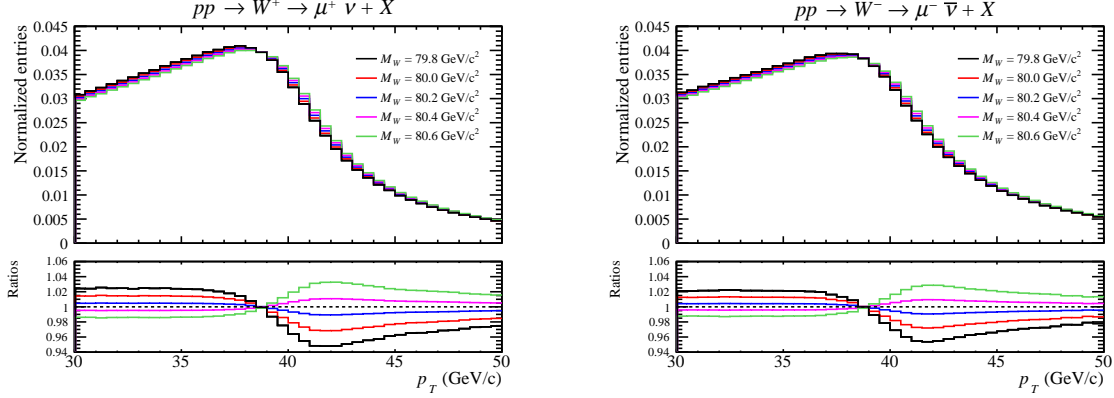


Figure 1: The simulated muon p_T distributions in $W \rightarrow \mu\nu$ decays with five different M_W hypotheses. The ratios are with respect to the prediction with $M_W = 80.3 \text{ GeV}/c^2$.

where M_W and Γ_W are the mass and the width of the W , respectively. The events are generated with a nominal value of M_W [2] but can be reweighted according to Eq. 1 to emulate a different M_W hypothesis. Fig. 1 shows how the shape of the p_T spectrum is distorted by variations in M_W .

A similar set of weights can be assigned to map the sample to different PDFs. As in [16] the full PDF uncertainty should consider an envelope of PDF sets from several groups, including for example the MMHT14 set [23], but for the current study we focus on the NNPDF3.1 [24] set with 1000 equiprobable *replicas*. The `pdfreweight` feature of POWHEG is used to generate a set of event weights that map between the different replicas.

3 Fitting method

Scaling the generated event samples to the 6 fb^{-1} of LHCb Run 2 data yields an expectation of 7.2 (4.8) million W^+ (W^-) events in the $30 < p_T < 50 \text{ GeV}/c$ and $2 < \eta < 4.5$ region. Toy data histograms are generated by randomly fluctuating the bins around the nominal distribution, assuming these yields and Poisson statistics. These histograms can be generated with different PDF sets using the reweighting procedure already described. The current study neglects experimental systematic uncertainties, such as those due to the knowledge of the momentum scale and the dependence of the muon identification efficiency on p_T and η , and does not address the systematic uncertainties related to the p_T^W modelling.

The data histograms are compared to templates with different PDF and M_W hypotheses. The normalisation of each template is scaled to match the data such that the fit only considers the shape information. For a given PDF hypothesis a simple single-parameter fit determines the value of M_W that minimises the χ^2 between a toy and the templates. The 68% C.L. statistical uncertainty corresponds to a variation of $\Delta\chi^2 = 1$ with respect to the parabola minimum.

Fig. 2 shows, separately for the two W charges, how the results of a fit to a single toy dataset vary with the PDF replica used in the templates. The M_W values follow approximately Gaussian distributions with widths of 15 (20) MeV/c^2 for the W^+ (W^-).

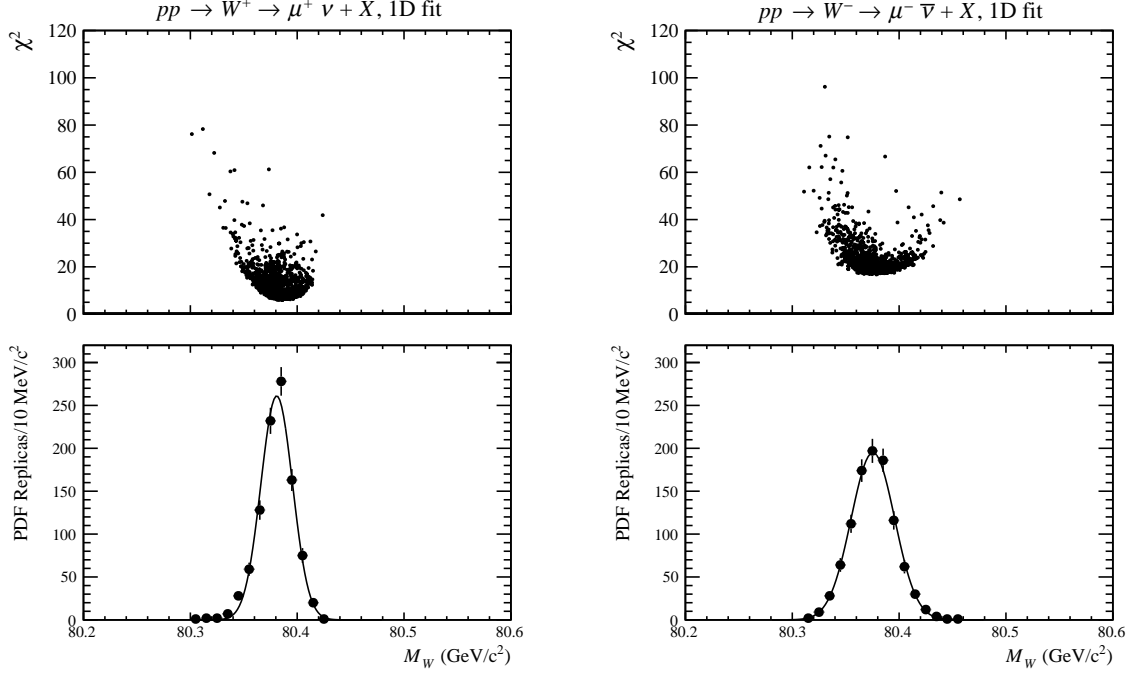


Figure 2: Upper: the distribution of the χ^2 versus M_W for a fit to a single toy dataset, which assumes the LHCb Run 2 statistics, with each of the 1000 NNPDF3.1 replicas. Lower: the distribution of the M_W values with a Gaussian fit function overlaid.

The broadly parabolic distributions of the fit χ^2 versus M_W indicate that the PDF replicas that most severely bias M_W tend to give a measurably poorer fit quality. Before evaluating how this information could be used to constrain the PDF uncertainty let us first try to understand in more detail the underlying mechanism behind the PDF uncertainty.

4 Importance of PDF regions

Fig. 3 shows how the different partonic subprocesses contribute to the cross-section for W production as a function of rapidity (y). The dominant $W^+(W^-)$ production subprocesses involve valence $u(d)$ quarks, while contributions from second generation quarks are below 10% or so. Fig. 4 shows the parton flavour composition as a function of Bjorken x . There is a clear dominance of valence $u(d)$ quarks as the higher x parton in $W^+(W^-)$ production. The lower x parton is usually a $\bar{d}(\bar{u})$ sea quark in $W^+(W^-)$ production, but there is also a sizeable contribution from gluons, particularly in the W^- case.

Since the u , \bar{d} , d and \bar{u} species seem to be the most important it is interesting to see if there are any obvious patterns in their respective PDFs for the replicas corresponding to biased M_W determinations. Fig. 5 show how the x dependencies of the u , \bar{d} , d and \bar{u} PDFs vary between the first 100 replicas. Each line is a ratio with respect to the central replica, and is assigned a colour according to the bias in M_W as evaluated using the method described in Sect. 3. No obvious patterns can be seen in the u and \bar{d} PDFs, which dominate W^+ production. However, a clear pattern can be seen for the high- x (above $x \sim 0.1$) d PDF, whereby the replicas that tend to bias M_W upwards(downwards) tend to have a smaller(larger) parton density. A qualitatively similar pattern, though with the

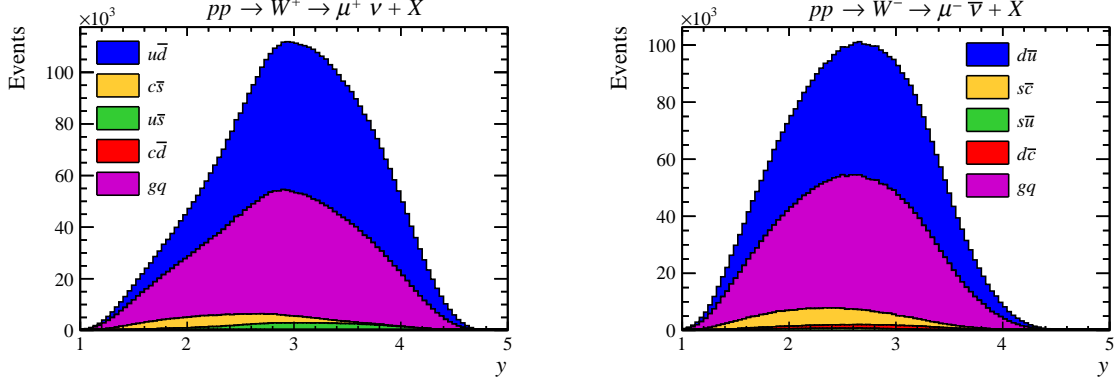


Figure 3: The (left) W^+ and (right) W^- rapidity distributions decomposed into the main partonic subprocesses.

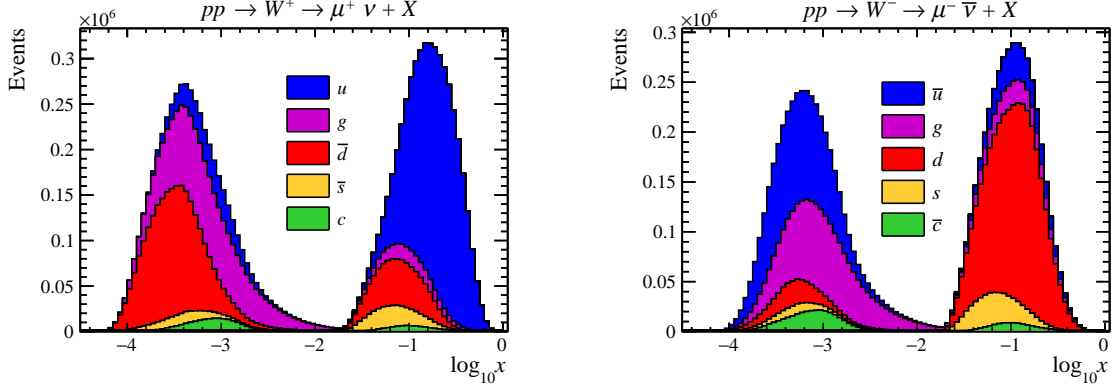


Figure 4: The Bjorken x distributions of the partons involved in the (left) W^+ and (right) (W^-) hard processes. The main parton species are stacked upon each other.

opposite sign, is seen in the \bar{u} PDF.

5 The role of the W kinematics

The PDF uncertainty on the M_W measurement arises because the p_T distribution depends on the W production kinematics, which are characterised by the transverse momentum (p_T^W), rapidity and polarisation. As a proxy for the polarisation, the angle θ^* in the Collins-Soper frame [25] can be considered. Fig. 6 shows how the p_T^W , y and $\cos\theta^*$ distributions vary between the first 100 NNPDF3.1 replicas. Each line is assigned a colour according to the bias in M_W for that replica. The underlying shapes of the distributions are also indicated by the filled histograms. A particularly striking pattern can be seen in the variation of the y distributions. The replicas that bias M_W upwards(downwards) tend to enhance(suppress) the W^+ cross-section at large rapidities. The opposite is seen for the W^- . Other clear patterns, though with smaller absolute variations, can be seen in the p_T^W and $\cos\theta^*$ projections. It is instructive to consider the two-dimensional projections of these patterns. Fig. 7 shows the mean of the y distribution versus the mean of the p_T^W distribution. Each point represents a single NNPDF3.1 replica using the already described

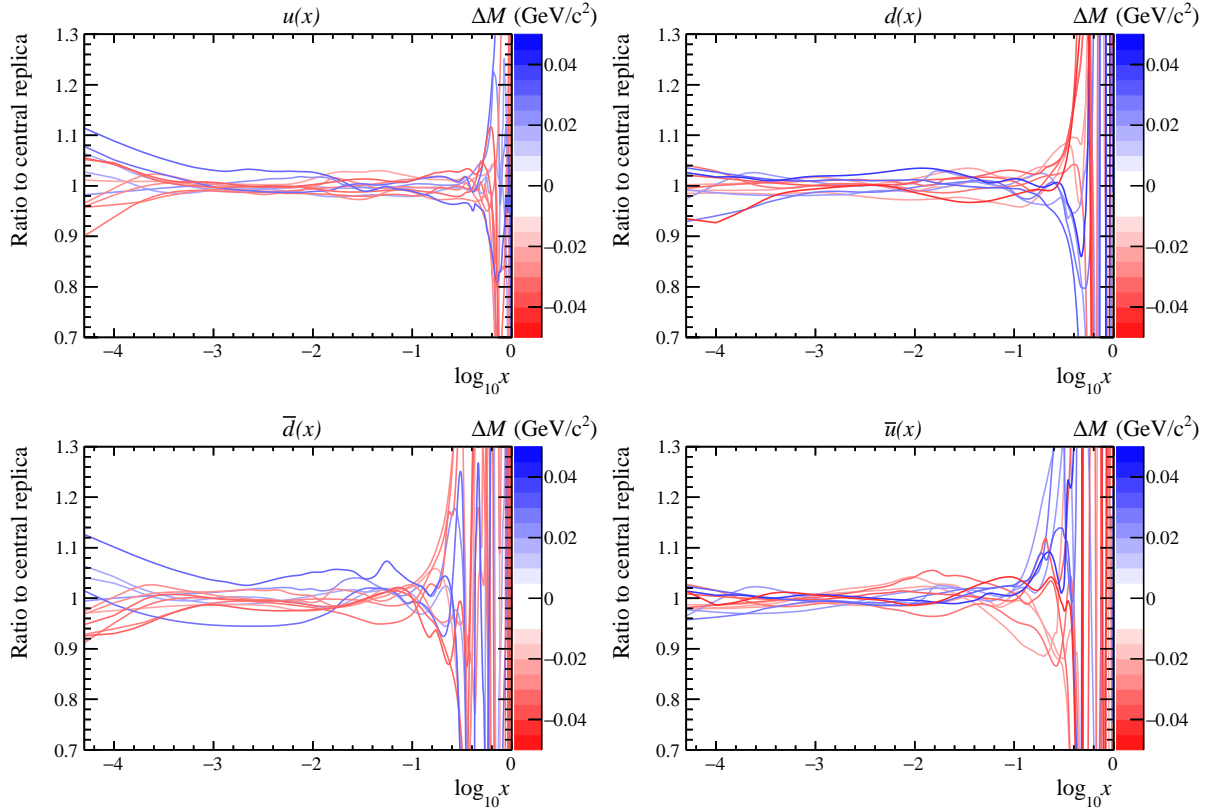


Figure 5: The ratios of the first 100 d and \bar{u} NNPDF3.1 replicas with respect to the central replica, for the x dependence of the (clockwise from upper left) u , d , \bar{u} and \bar{d} PDFs. Each line is marked with a colour indicating the shift of the M_W value determined from a fit to the p_T distribution of a single toy dataset.

M_W dependent colour scale. There is a clear anticorrelation between the changes in the shapes of the y and p_T^W distributions, but further patterns can be seen in the colour distribution. In the W^+ case, the replicas that bias M_W upwards(downwards) tend to predict larger(smaller) $\langle y \rangle$ values and smaller(larger) $\langle p_T^W \rangle$ values. The opposite pattern is seen for the W^- case. These striking patterns are helpful in understanding how biases in M_W are correlated with changes in the underlying W production kinematics.

Our attention is now switched to the muon kinematic distributions, encouraged by interesting studies on disentangling the W kinematics from the measurable muon observables in the ATLAS/CMS acceptance [26]. Fig. 8 shows how the muon p_T and η distributions vary with the PDF replicas. As expected the replicas that bias M_W upwards(downwards) correspond to a decrease(increase) in the predicted cross-section at high p_T with respect to low p_T . An intriguing observation, however, is that the problematic replicas cause a correlated change in the shape of the η distribution. This is a *measurable* change of up to several percent, which could be exploited to constrain the PDF uncertainty. Fig. 9 shows the mean p_T versus the mean η for each replica, with the M_W dependent colour scale as before. The replicas that bias M_W tend to be clearly separated in this two-dimensional plane, which encourages us to consider exploiting this information to constrain the PDF uncertainty.

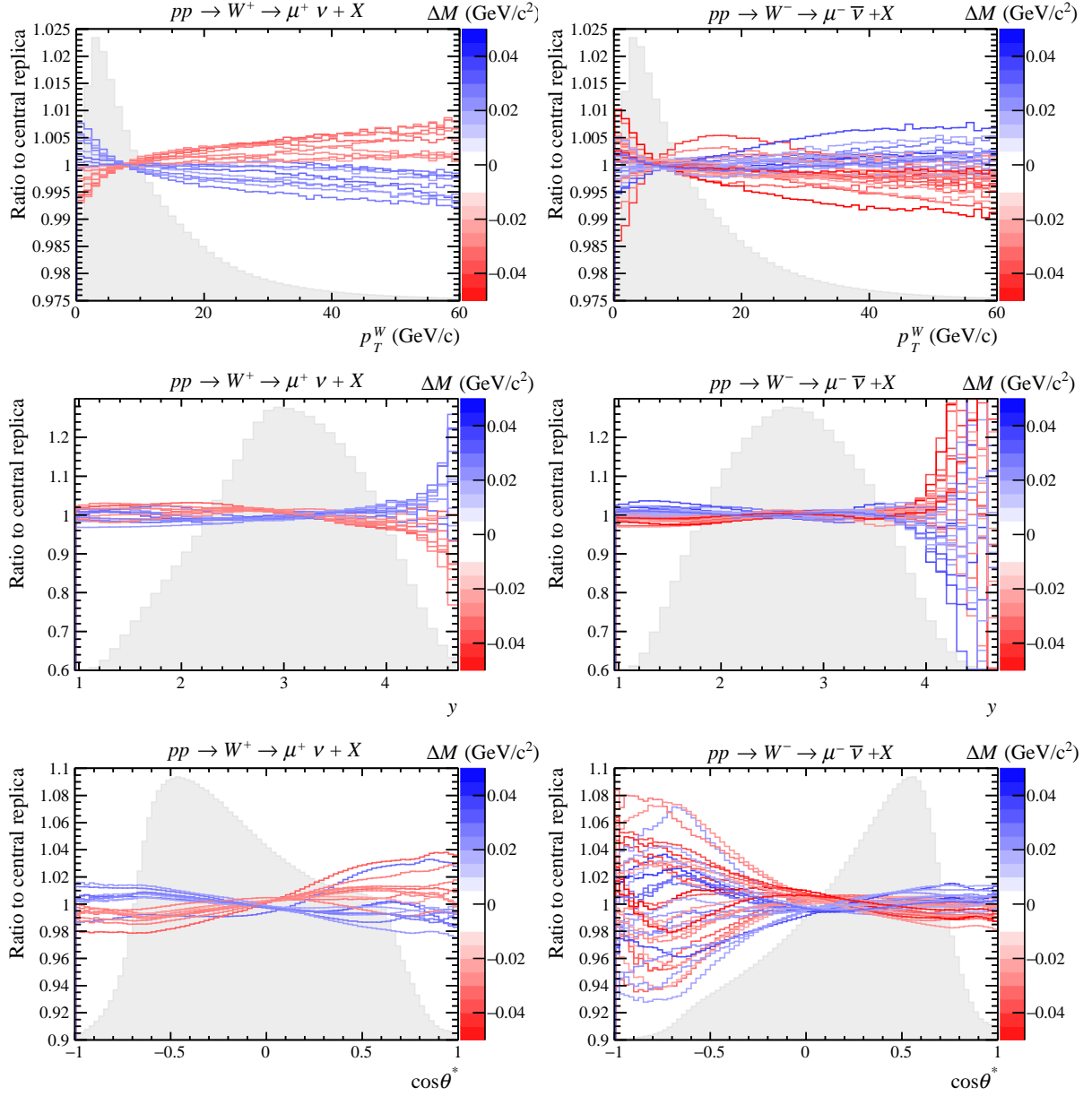


Figure 6: The variations in the shapes of the p_T^W , y and $\cos\theta^*$ distributions predicted with the first 100 NNPDF3.1 replicas. Each line is marked with a colour indicating the shift of the M_W value determined from a fit to the p_T distribution of a single toy dataset. For clarity, the replicas for which the shift in M_W is close to zero are not drawn.

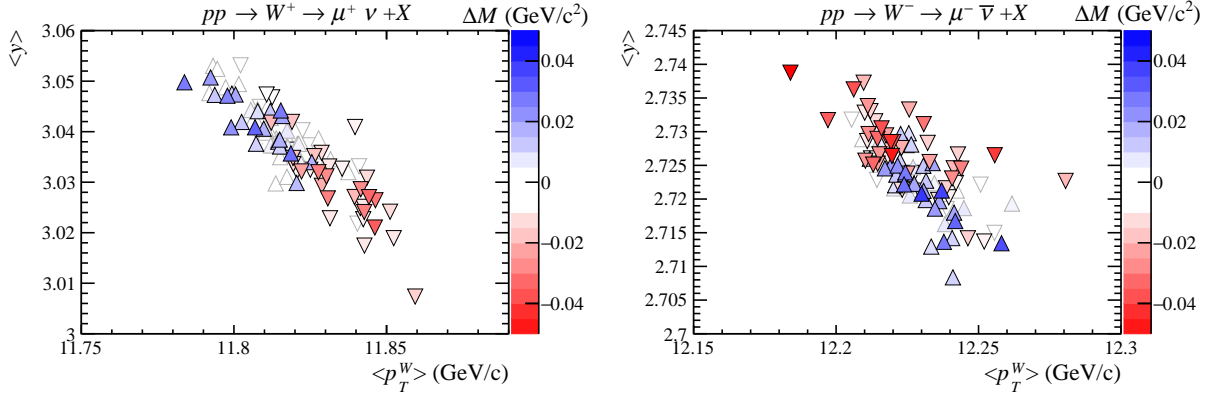


Figure 7: The distributions of $\langle p_T^W \rangle$ and $\langle y \rangle$ for the first 100 replicas of the NNPDF3.1 set. Each marker is assigned a colour according to the shift of the M_W value determined from a fit to the p_T distribution of a single toy dataset. The markers drawn with an up(down) pointing triangle correspond to ΔM values greater(less) than zero.

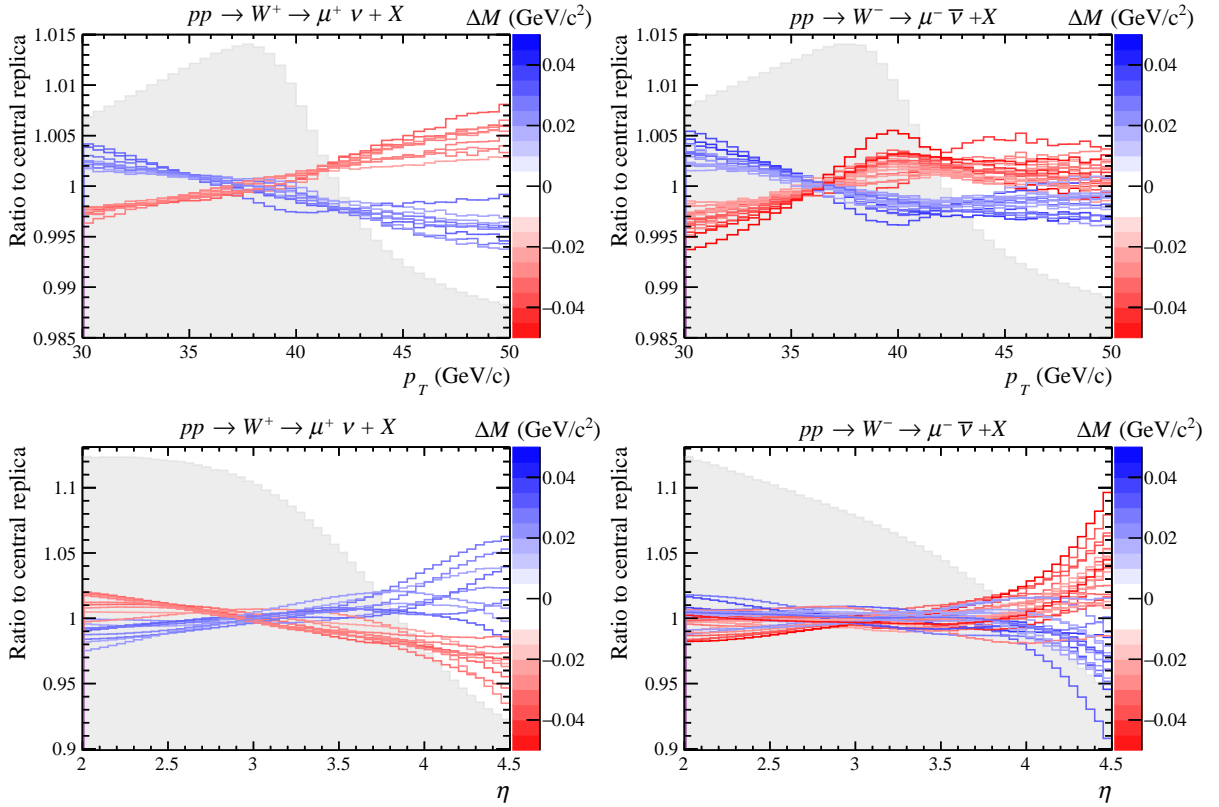


Figure 8: The variations in the shapes of the p_T and η distributions predicted with the first 100 NNPDF3.1 replicas. Each line is marked with a colour indicating the shift of the M_W value determined from a fit to the p_T distribution of a single toy dataset. For clarity, the replicas for which the shift in M_W is close to zero are not drawn.

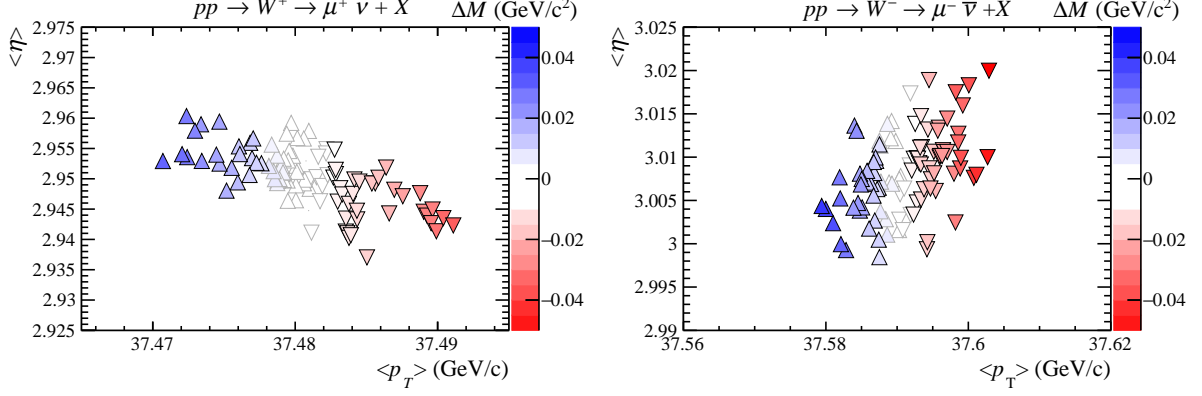


Figure 9: The distribution of $\langle p_T \rangle$ and $\langle \eta \rangle$ produced using the first 100 replicas of the NNPDF3.1 set and divided by the central replica. Each marker is assigned a colour according to the shift of the M_W value determined from a fit to the p_T distribution of a single toy dataset. The markers drawn with an up(down) pointing triangle correspond to ΔM values greater(less) than zero.

6 PDF uncertainty reduction

In Sect. 3 it was noted that the traditional one-dimensional fit to the p_T distribution already suggests a potential for *in situ* constraint of the PDF uncertainty [27]. However, Sect. 5 encourages the consideration of a fit to the two-dimensional (p_T versus η) distribution. One-dimensional and two-dimensional fits are now compared with and without the inclusion of replica weights. Using the NNPDF prescription [28, 29], each replica is assigned a weight according to the χ^2 for a fit with n degrees of freedom (n):

$$P(\chi^2) \propto \chi^{n-1} e^{-\frac{1}{2}\chi^2}. \quad (2)$$

This has the effect of disregarding replicas that are incompatible with the data. The two-dimensional fit uses three bins in η within the ($2 < \eta < 4.5$) range already described. Fig. 10 shows, separately for the W^+ and W^- cases, the distribution of M_W and χ^2 values for the two-dimensional fit to a single toy dataset. The distributions of M_W values are shown with and without the replica weights. In the W^+ case the width of weighted distribution is roughly a factor of three smaller than the unweighted distribution. For the W^- the width is reduced by roughly 50%.

The weights are clearly dependent on the toy data, so it is now important to consider the results with multiple toy datasets. For a single toy dataset the PDF uncertainty is defined by the RMS of the M_W values for the 1000 replicas. Fig. 11 shows the distribution of the PDF uncertainty for 1000 toy datasets, comparing the one-dimensional fit with and without weights, and the two-dimensional fit with weights. In the one-dimensional case the weighting reduces the uncertainty by a typical factor of 10-30% (10-70%) for the W^+ (W^-). The two-dimensional weighted case corresponds to a most probable improvement by a factor of roughly two (1.5) for the W^+ (W^-). These encouraging results strongly motivate the adoption of the two-dimensional fit method by LHCb.

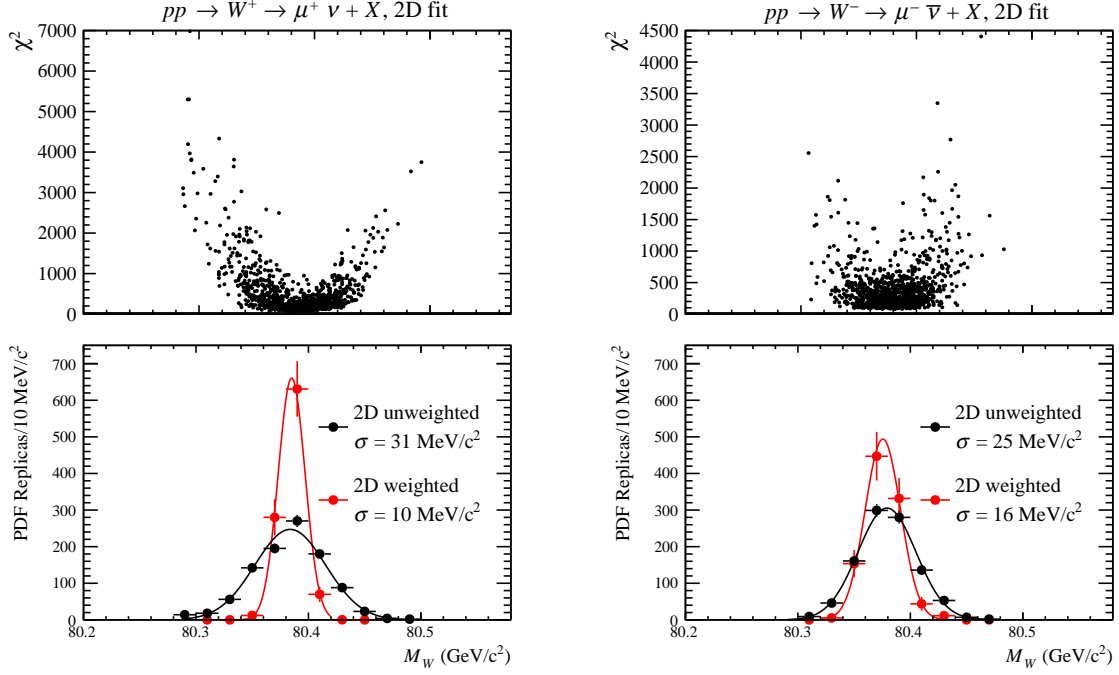


Figure 10: Upper: the distribution of the χ^2 versus M_W for a two-dimensional fit to a single toy dataset, which assumes the LHCb Run 2 statistics, with each of the 1000 NNPDF3.1 replicas. Lower: the distribution of the extracted M_W values, with a Gaussian fit function overlaid, without (black) and with (red) weighting.

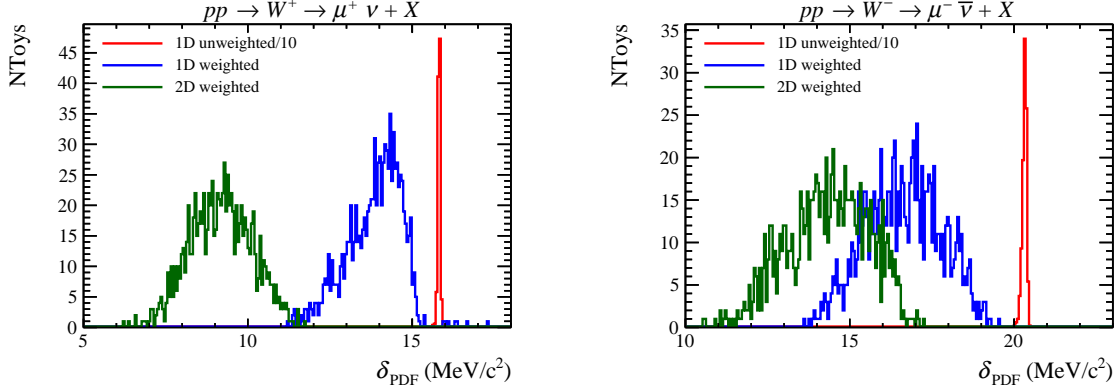


Figure 11: The distribution of the PDF uncertainty evaluated for 1000 toy datasets using three different methods: p_T fit without weighting, p_T fit with weighting, (p_T, η) fit with weighting. The one-dimensional unweighted distribution is arbitrarily scaled down by a factor of ten.

7 Simultaneous fit of W^+ and W^- samples

Following the promising results shown for separate fits to the W^+ and W^- data it is now interesting to consider the combination of the two charges. Fig. 12 shows, separately for the one-dimensional and two-dimensional approaches, the W^+ versus W^- fit results for a single toy dataset. Each point represents a different PDF replica. Interestingly, for both fit approaches, there is a clear negative correlation, which implies a partial cancellation of

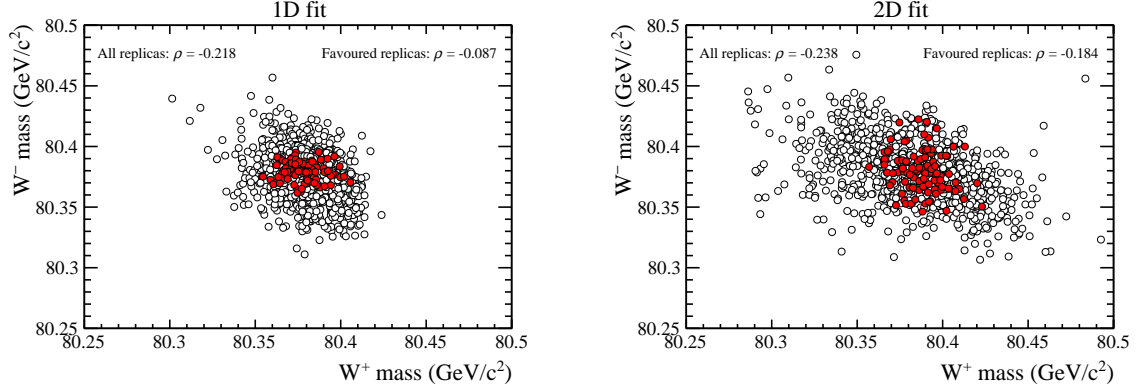


Figure 12: The distribution of the W^- versus W^+ mass determined from a single toy dataset with each of the NNPDF3.1 replicas. Ten percent of the replicas with the highest $P(\chi^2)$ (product over the two W charges) are assigned red markers.

the PDF uncertainty when the W^+ and W^- data are combined. It is now interesting to see how this partial anti-correlation is affected by (i) the weights and (ii) moving to a two-dimensional fit. Therefore, in Fig. 12 ten percent of the points corresponding to the largest product (over the two W charges) of $P(\chi^2)$ values are highlighted. Unfortunately, in both the one- and two-dimensional fit cases, the subset of favoured replicas exhibits a correlation coefficient with a reduced magnitude. Before attempting to perform a fit to the combined W^+ and W^- data there is a further consideration. Fig. 13 shows the variation between the replicas of the charge asymmetry between the W^+ and W^- cross sections, as a function of η . The lines are assigned a colour according to the shift in the M_W value determined in a simultaneous fit (one-dimensional) of the W^+ and W^- data. A clear pattern can be seen whereby replicas that bias M_W upwards(downwards) tend to shift the charge asymmetry upwards(downwards), particularly at large η values. Most of the η dependence is already taken into account with the weighted two-dimensional fit, but the integrated charge asymmetry can be trivially included as a constraint by sharing the normalisation factor between the two W charges. Fig. 14 shows the χ^2 versus M_W values for combined (W^+ and W^-) fits to a single toy dataset. Each point corresponds to a different NNPDF3.1 replica, and the results are shown separately for the one-dimensional and two-dimensional fits. The weighted and unweighted M_W distributions are shown with corresponding Gaussian fits overlaid. With these data the weights have very little effect on the width of the distribution in the one-dimensional case. In the two-dimensional case, however, there is roughly a factor of two of improvement.

Fig. 15 (left) shows the distribution of the PDF uncertainty in 1000 toy datasets, in combined fits of the W^+ and W^- data. Compared to the traditional one-dimensional fit, the addition of the weighting typically improves the PDF uncertainty by around 10%. The two-dimensional fit with weighting is, however, typically around a factor of two better. If the normalisation is no longer shared between the W^+ and W^- the uncertainty is typically slightly larger, but this change is usually less than 1 MeV. Fig. 15 (right) considers an alternative approach whereby the W^+ and W^- data are analysed separately, and the corresponding M_W values are combined in a weighted average. This results in larger uncertainties, and therefore encourages the simultaneous fit of W^+ and W^- data with a single shared M_W fit parameter.

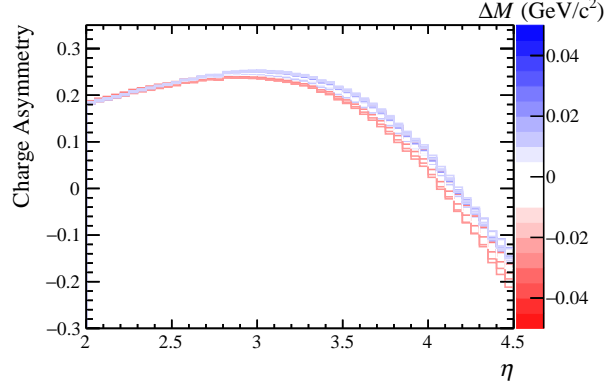


Figure 13: The charge asymmetry as a function of η for the first 100 NNPDF3.1 replicas. The colour scale indicates the shift of the M_W value extracted for each replica with respect to the central replica using a simultaneous one-dimensional fit of W^+ and W^- samples.

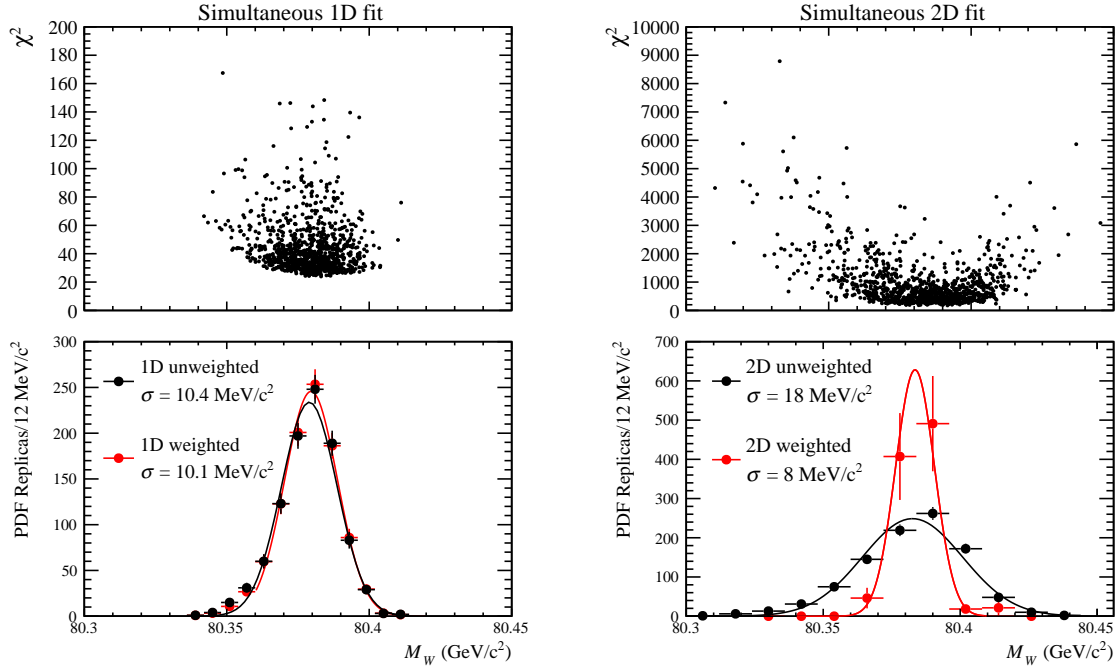


Figure 14: Upper: the distribution of χ^2 versus M_W for a one-dimensional (left) and two-dimensional (right) simultaneous fit to a single toy dataset, which assumes the LHCb Run 2 statistics, with each of the 1000 NNPDF3.1 replicas. Lower: the extracted M_W values, with a Gaussian fit function overlaid, without (black) and with (red) weighting. In the simultaneous fit the W^+ and W^- templates share the same normalisation.

8 Dependence on the detector acceptance

The study has thus far restricted to events in the range $30 < p_T < 50$ GeV/c and $2 < \eta < 4.5$. It is interesting to now consider how the results depend on this choice, since the LHCb acceptance extends slightly outside this eta range, and LHCb is able to trigger on muons with far smaller p_T values without any prescales. Fig. 16 shows how the

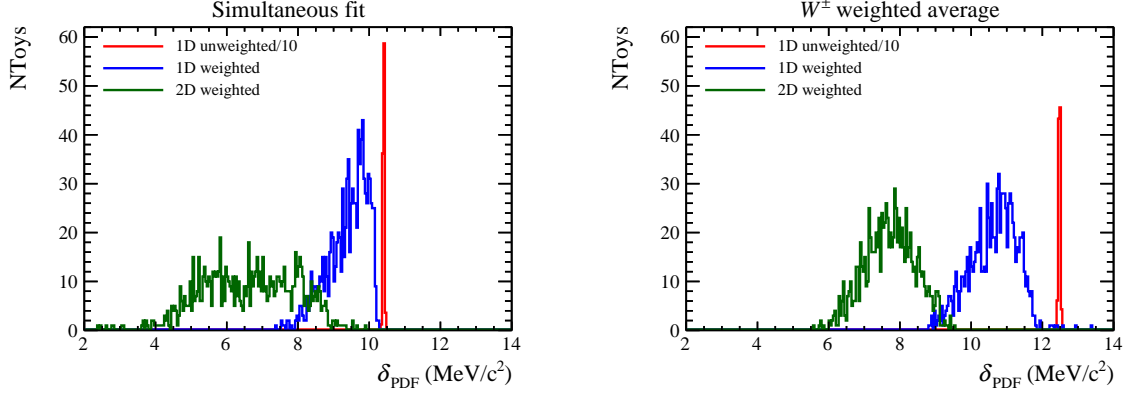


Figure 15: The distribution of the PDF uncertainty evaluated for 1000 toy datasets from (left) a simultaneous fit where the W^+ and W^- templates share the same normalisation or (right) a weighted average of single W charges measurements. Three different fit methods are compared: p_T fit without weighting, p_T fit with weighting, (p_T, η) fit with weighting. The one-dimensional unweighted distribution is arbitrarily scaled down by a factor of ten.

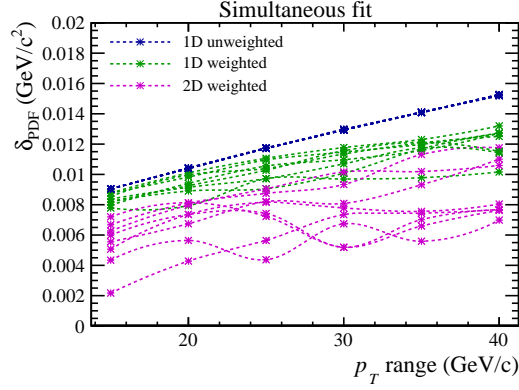


Figure 16: PDF uncertainty as a function of the p_T range used in the simultaneous fit, evaluated for several toy datasets. The η range is set to $2 < \eta < 4.5$. In the two dimensional fits three η bins are used.

PDF uncertainties depend on the width of the p_T interval, which is symmetric around $M_W/2$. The results for several toy datasets are shown. With the simple one-dimensional unweighted fit the PDF uncertainty grows approximately linearly with the width of the p_T interval. This is also the case for the one- and two-dimensional weighted fits, though the slope is less severe. Fig. 17 considers separately the dependence on the minimum and maximum η value. The uncertainty is found to reduce when the η range is extended in either direction. The uncertainty is not significantly changed if the number of η bins is increased from the nominal value of three. Using only three bins in η should make the experimental control of the η dependence of the muon efficiency more straightforward to control than if more bins are required.

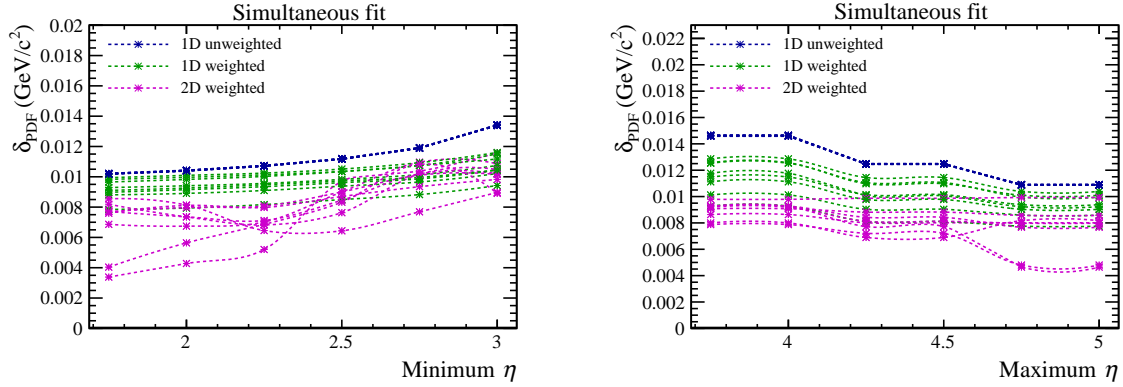


Figure 17: PDF uncertainty as a function of the lower(left) and upper(right) η cut used in the simultaneous fit, evaluated for several toy datasets. The p_T is in the range $30 < p_T < 50$ GeV/c. Left(Right): the upper(lower) η cut set to 4.5(2). In the two dimensional fits three η bins are used.

9 Conclusions

It has recently been suggested that LHCb should perform a measurement of M_W based on a one-dimensional fit to the muon p_T distribution in samples of $W \rightarrow \mu\nu$ decays. Thanks to LHCb's unique angular coverage this measurement would complement those performed by ATLAS and CMS, particularly when considering PDF uncertainties. Here we report on a detailed study of the PDF uncertainty, restricting to the NNPDF3.1 set, on the proposed LHCb measurement. It is found that the variations in the PDFs that tend to bias the determination of M_W lead to clear patterns of variation in the shapes of the W kinematic distributions, in particular the rapidity distribution. A particularly interesting observation is that those variations also lead to a *measurable* change in the shape of the muon η distribution. Given that the PDF variations also fail to perfectly mimic a change in M_W in the p_T spectrum, this suggests that a two-dimensional fit to the p_T versus η distribution, with PDF replica weighting, would allow the PDF uncertainty to be constrained. A study with 1000 toy experiments, assuming the LHCb Run 2 statistics, indicates a typical improvement of around a factor of two, compared to the one-dimensional unweighted fit, when fitting the W^+ and W^- data simultaneously. The full PDF uncertainty should also include the variation between results from different PDF fitting groups, but this is a very encouraging result. In order to facilitate the study of the possible impact of other data a table of M_W biases for the first 100 NNPDF3.1 replicas is provided as supplementary material. The main study considers events in which the muon satisfies $2 < \eta < 4.5$ and $30 < p_T < 50$, but the dependence on these choices is also studied since there are likely to be many considerations on the optimal fit range for the real measurement.

Acknowledgements

We thank W. Barter, M. Charles, G. Bozzi, A. Vicini, A. Cooper-Sakar, L. Harland-Lang and J. Rojo for their helpful comments and suggestions during the preparation of this manuscript. OL thanks the CERN LBD group for their support during the period when most of this work was carried out, and MV thanks the Science and Technologies Facilities

Council for their support through an Ernest Rutherford Fellowship.

References

- [1] J. Haller *et al.*, *Update of the global electroweak fit and constraints on two-Higgs-doublet models*, Eur. Phys. J. **C78** (2018), no. 8 675, [arXiv:1803.01853](#).
- [2] Particle Data Group, C. Patrignani *et al.*, *Review of Particle Physics*, Chin. Phys. **C40** (2016), no. 10 100001.
- [3] CDF, T. Aaltonen *et al.*, *Precise measurement of the W -boson mass with the CDF II detector*, Phys. Rev. Lett. **108** (2012) 151803, [arXiv:1203.0275](#).
- [4] D0, V. M. Abazov *et al.*, *Measurement of the W Boson Mass with the D0 Detector*, Phys. Rev. Lett. **108** (2012) 151804, [arXiv:1203.0293](#).
- [5] D0, V. M. Abazov *et al.*, *Measurement of the W Boson Mass with the D0 Detector*, Phys. Rev. Lett. **108** (2012) 151804, [arXiv:1203.0293](#).
- [6] M. W. Krasny *et al.*, $\Delta M_W \leq 10 \text{ MeV}/c^2$ at the LHC: a forlorn hope?, Eur. Phys. J. **C69** (2010) 379, [arXiv:1004.2597](#).
- [7] G. Bozzi, J. Rojo, and A. Vicini, *The Impact of PDF uncertainties on the measurement of the W boson mass at the Tevatron and the LHC*, Phys. Rev. **D83** (2011) 113008, [arXiv:1104.2056](#).
- [8] J. Rojo and A. Vicini, *PDF uncertainties in the extraction of the W mass at LHC: a Snowmass Whitepaper*, in *Proceedings, 2013 Community Summer Study on the Future of U.S. Particle Physics: Snowmass on the Mississippi (CSS2013): Minneapolis, MN, USA, July 29-August 6, 2013*, 2013. [arXiv:1309.1311](#).
- [9] G. Bozzi, L. Citelli, and A. Vicini, *Parton density function uncertainties on the W boson mass measurement from the lepton transverse momentum distribution*, Phys. Rev. **D91** (2015), no. 11 113005, [arXiv:1501.05587](#).
- [10] S. Quackenbush and Z. Sullivan, *Parton distributions and the W mass measurement*, Phys. Rev. **D92** (2015), no. 3 033008, [arXiv:1502.04671](#).
- [11] ATLAS, M. Aaboud *et al.*, *Measurement of the W -boson mass in pp collisions at $\sqrt{s} = 7 \text{ TeV}$ with the ATLAS detector*, Eur. Phys. J. **C78** (2018), no. 2 110, [arXiv:1701.07240](#), [Erratum: Eur. Phys. J. **C78**, no. 11, 898 (2018)].
- [12] LHCb, R. Aaij *et al.*, *LHCb Detector Performance*, Int. J. Mod. Phys. **A30** (2015), no. 07 1530022, [arXiv:1412.6352](#).
- [13] LHCb, R. Aaij *et al.*, *Measurement of forward W and Z boson production in pp collisions at $\sqrt{s} = 8 \text{ TeV}$* , JHEP **01** (2016) 155, [arXiv:1511.08039](#).
- [14] LHCb, R. Aaij *et al.*, *Measurement of the forward Z boson production cross-section in pp collisions at $\sqrt{s} = 13 \text{ TeV}$* , JHEP **09** (2016) 136, [arXiv:1607.06495](#).

- [15] LHCb, R. Aaij *et al.*, *Measurement of the forward-backward asymmetry in $Z/\gamma^* \rightarrow \mu^+\mu^-$ decays and determination of the effective weak mixing angle*, JHEP **11** (2015) 190, [arXiv:1509.07645](#).
- [16] G. Bozzi, L. Citelli, M. Vesterinen, and A. Vicini, *Prospects for improving the LHC W boson mass measurement with forward muons*, Eur. Phys. J. **C75** (2015), no. 12 601, [arXiv:1508.06954](#).
- [17] ATLAS, *Prospects for the measurement of the W -boson mass at the HL- and HE-LHC*, Tech. Rep. ATL-PHYS-PUB-2018-026, CERN.
- [18] *Impact of the LHCb upgrade detector design choices on physics and trigger performance*, Tech. Rep. LHCb-PUB-2014-040, CERN.
- [19] LHCb, R. Aaij *et al.*, *Physics case for an LHCb Upgrade II - Opportunities in flavour physics, and beyond, in the HL-LHC era*, [arXiv:1808.08865](#).
- [20] S. Alioli, P. Nason, C. Oleari, and E. Re, *NLO vector-boson production matched with shower in POWHEG*, JHEP **07** (2008) 060, [arXiv:0805.4802](#).
- [21] J. Gao *et al.*, *CT10 next-to-next-to-leading order global analysis of QCD*, Phys. Rev. **D89** (2014), no. 3 033009, [arXiv:1302.6246](#).
- [22] T. Sjostrand, S. Mrenna, and P. Z. Skands, *PYTHIA 6.4 Physics and Manual*, JHEP **05** (2006) 026, [arXiv:hep-ph/0603175](#).
- [23] L. A. Harland-Lang, A. D. Martin, P. Motylinski, and R. S. Thorne, *Parton distributions in the LHC era: MMHT 2014 PDFs*, Eur. Phys. J. **C75** (2015), no. 5 204, [arXiv:1412.3989](#).
- [24] NNPDF, R. D. Ball *et al.*, *Parton distributions from high-precision collider data*, Eur. Phys. J. **C77** (2017), no. 10 663, [arXiv:1706.00428](#).
- [25] J. C. Collins and D. E. Soper, *Angular Distribution of Dileptons in High-Energy Hadron Collisions*, Phys. Rev. **D16** (1977) 2219.
- [26] E. Manca, O. Cerri, N. Foppiani, and G. Rolandi, *About the rapidity and helicity distributions of the W bosons produced at LHC*, JHEP **12** (2017) 130, [arXiv:1707.09344](#).
- [27] W. T. Giele and S. Keller, *Implications of hadron collider observables on parton distribution function uncertainties*, Phys. Rev. **D58** (1998) 094023, [arXiv:hep-ph/9803393](#).
- [28] NNPDF, R. D. Ball *et al.*, *Reweighting NNPDFs: the W lepton asymmetry*, Nucl. Phys. **B849** (2011) 112, [arXiv:1012.0836](#), [Erratum: Nucl. Phys. **B855**, 927(2012)].
- [29] R. D. Ball *et al.*, *Reweighting and Unweighting of Parton Distributions and the LHC W lepton asymmetry data*, Nucl. Phys. **B855** (2012) 608, [arXiv:1108.1758](#).

Additional material

	ΔM_+ (GeV/ c^2)		ΔM_- (GeV/ c^2)		ΔM_s (GeV/ c^2)	
$R_{\text{NNPDF3.1}}$	1D fit	2D fit	1D fit	2D fit	1D fit	2D fit
1	0.004	0.0191	0.0159	0.0134	0.008	0.0172
2	0.0195	0.0169	-0.0349	-0.0378	0.0007	-0.0011
3	-0.0074	-0.0247	-0.0063	0.0012	-0.007	-0.0163
4	0.0071	-0.0015	0.0392	0.0438	0.0181	0.0133
5	-0.0068	-0.0057	-0.0164	-0.0141	-0.0101	-0.0085
6	0.0032	-0.0043	0.0053	0.0077	0.0039	-0.0004
7	0.0049	-0.0051	-0.0048	-0.0087	0.0015	-0.0064
8	0.011	0.0174	-0.0119	-0.0183	0.0031	0.0057
9	0.0057	0.0392	0.0072	-0.0048	0.0062	0.0248
10	-0.0077	-0.0402	-0.0015	0.0019	-0.0056	-0.0264
11	0.0077	0.0248	-0.0158	-0.0213	-0.0004	0.0096
12	-0.0168	-0.0353	-0.0076	-0.0107	-0.0137	-0.0273
13	-0.012	-0.014	-0.0134	-0.0117	-0.0125	-0.0133
14	0.0087	0.0165	-0.0197	-0.028	-0.0011	0.0018
15	-0.0308	-0.0611	-0.0133	-0.0141	-0.0248	-0.0457
16	-0.0063	-0.0268	0.0152	0.0247	0.001	-0.01
17	-0.0103	-0.0359	-0.0033	0.4204	-0.0079	-0.0229
18	0.02	0.0266	-0.0307	-0.0467	0.0025	0.0024
19	0.0037	-0.015	-0.0106	-0.0046	-0.0012	-0.0116
20	-0.0002	-0.0045	-0.0382	-0.0405	-0.0133	-0.0164
21	-0.029	-0.0688	0.0082	0.0226	-0.0162	-0.0389
22	0.0166	0.0233	0.0011	-0.0003	0.0112	0.0155
23	0.0204	0.0333	-0.0287	-0.0364	0.0035	0.0104
24	0.0185	0.0279	-0.021	-0.0313	0.005	0.0084
25	0.0027	0.0287	0.0045	-0.0054	0.0033	0.0174
26	-0.0036	0.007	0.0331	0.0492	0.009	0.0208
27	-0.0191	-0.0289	-0.0195	-0.0188	-0.0193	-0.0256
28	-0.0056	0.008	-0.0082	-0.0161	-0.0065	-0.0073
29	0.016	0.012	0.0221	0.4204	0.0076	0.0156
30	0.0149	0.036	0.0147	0.0106	0.4214	0.418
31	0.0246	0.0389	-0.0305	-0.0375	0.0057	0.0138
32	-0.0101	-0.0299	0.0078	0.0152	-0.004	-0.0152
33	0.0304	0.0531	-0.0167	-0.0323	0.0141	0.0248
34	-0.0255	-0.0445	0.0231	0.0329	-0.0088	-0.0191
35	-0.0214	-0.0307	0.0053	-0.0038	-0.0122	-0.0219
36	-0.0021	-0.0043	0.0404	0.0467	0.0125	0.0123
37	0.0324	0.0365	-0.0085	-0.0079	0.0183	0.0219
38	-0.0054	-0.0005	-0.0139	-0.0122	-0.0084	-0.0044
39	0.0141	0.0433	-0.0321	-0.0475	-0.0018	0.0132
40	-0.0327	-0.0576	-0.0052	-0.0203	-0.0232	-0.0454
41	-0.0171	-0.0141	0.0175	0.0181	-0.0052	-0.0036
42	-0.0142	-0.0189	0.0127	0.0147	-0.005	-0.0079
43	0.0061	0.0172	-0.0212	-0.0281	-0.0033	0.0022
44	0.0095	0.018	-0.0218	-0.0291	-0.0012	0.0025
45	0.0055	0.0025	0.0064	0.0081	0.0058	0.0043
46	-0.0262	-0.0478	0.0297	0.0429	-0.007	-0.0182
47	-0.0121	-0.0528	-0.0415	-0.0398	-0.0224	-0.0486
48	-0.018	-0.028	0.0129	0.0234	0.0044	-0.0113
49	0.0021	-0.0017	-0.0131	-0.0144	-0.0032	-0.0059
50	0.0206	0.0618	-0.0353	-0.0511	0.0014	0.0244
51	0.0067	0.0151	-0.0086	-0.0126	0.0015	0.0059
52	-0.0155	-0.0152	0.0149	0.0163	-0.005	-0.0049
53	-0.0035	0.0127	0.0288	0.0316	0.0076	0.0189
54	-0.0254	-0.0514	-0.0278	-0.016	-0.0263	-0.0399
55	0.0055	0.0068	-0.0238	-0.0267	-0.0046	-0.0043
56	0.0032	0.0401	0.0035	-0.0028	0.0033	0.026
57	0.0129	0.0237	0.0217	0.0212	0.016	0.0228
58	0.0035	0.006	0.0155	0.0185	0.0076	0.0101
59	-0.0095	-0.0232	0.0131	0.0219	-0.0018	-0.0085
60	0.0156	0.0243	-0.0228	-0.0259	0.0024	0.0077
61	0.0281	0.0312	0.012	0.0055	0.0225	0.0227
62	-0.0065	-0.0032	0.0098	0.0018	-0.1034	-0.1068
63	0.0074	0.0155	0.013	0.0097	0.0093	0.0135
64	0.0283	0.0771	-0.0492	-0.0666	0.0016	0.0294
65	0.0042	-0.0175	-0.0252	-0.0297	-0.0059	-0.0215
66	-0.0004	-0.0015	0.0364	0.0427	0.0122	0.0129
67	0.0014	0.0235	0.0249	0.0154	0.0094	0.0208
68	0.0135	0.0357	-0.0249	-0.0352	0.0003	0.0123
69	0.0239	0.0523	-0.0081	-0.0206	0.0129	0.0283
70	0.0134	0.0304	-0.0225	-0.0264	0.001	0.0116
71	0.0073	0.0062	-0.012	-0.0226	0.0006	-0.0033
72	0.0057	0.0055	-0.0168	-0.0126	-0.0021	-0.0005
73	0.0073	0.0051	-0.0321	-0.0333	-0.0063	-0.0076
74	0.0055	0.0009	-0.0203	-0.0234	-0.0034	-0.0071
75	0.0139	0.0102	0.0115	0.0146	0.0131	0.0116
76	-0.0091	-0.0482	-0.0133	0.0021	-0.0105	-0.0317
77	0.0045	0.0161	0.0095	0.0094	0.0062	0.0138
78	-0.0054	-0.0064	0.0024	0.0024	-0.0028	-0.0036
79	0.0015	0.0008	0.0095	0.0025	0.0042	0.0013
80	-0.0274	-0.0431	0.0114	0.0111	-0.0141	-0.0253
81	-0.0018	-0.0217	-0.0147	0.0018	-0.0063	-0.014
82	-0.0145	-0.0203	0.0227	0.0271	-0.0017	-0.0048
83	-0.0001	-0.0404	0.0205	0.0301	0.007	-0.0173
84	-0.0088	-0.0383	0.0106	0.0312	-0.0021	-0.0155
85	-0.0276	-0.0562	-0.0062	-0.0035	-0.0203	-0.039
86	-0.0094	-0.0184	-0.003	0.0076	-0.0072	-0.0099
87	-0.0032	0.0105	0.0204	0.0173	0.0049	0.0127
88	0.0001	-0.0057	-0.0042	-0.0023	-0.0014	-0.0046
89	0.001	0.036	0.0235	0.0128	0.0087	0.0283
90	-0.0091	-0.0416	-0.0012	0.0066	-0.0064	-0.0258
91	0.0267	0.0642	-0.005	-0.0197	0.0158	0.0364
92	-0.0081	-0.0485	0.0011	0.0125	-0.0049	-0.0286
93	-0.0037	-0.0077	0.0214	0.0284	0.0049	0.0041
94	0.0083	0.0066	0.0158	0.0182	0.0108	0.0104
95	0.0052	0.0144	-0.006	-0.0069	0.0014	0.0073
96	-0.0026	-0.0041	-0.0457	-0.0504	-0.0174	-0.0194
97	0.0038	0.0209	-0.0088	-0.0125	-0.0006	0.0098
98	-0.0111	-0.0141	0.009	0.0169	-0.0042	-0.004
99	0.0025	0.0046	0.0309	0.0352	0.0122	0.0146
100	0.0082	0.0224	-0.0132	-0.0129	0.0008	0.0108

Table 1: Shift in the extracted M_W values for the first 100 NNPDF3.1 replicas with respect to the central replica. Both single W charges results and the simultaneous fit results are shown. The ΔM values are extracted from both the one-dimensional and the two-dimensional fit. In the simultaneous fit the normalisation constraint of the W^+ and W^- templates is taken into account.